PCCP

Experimental Phase Diagram and its Temporal Evolution for Submicron 2-Methylglutaric Acid and Ammonium Sulfate Aerosol Particles

Journal:	*Physical Chemistry Chemical Physics*
Manuscript ID	CP-ART-09-2023-004411.R1
Article Type:	Paper
Date Submitted by the Author:	03-Nov-2023
Complete List of Authors:	Huang, Qishen; The Pennsylvania State University, Chemistry; Beijing Institute of Technology, Chemistry and Chemical Engineering Pitta, Kiran; The Pennsylvania State University, Chemistry Constantini, Kayla; The Pennsylvania State University, Chemistry Ott, Emily; The Pennsylvania State University, Chemistry Zuend, Andreas; McGill University, Atmospheric and Oceanic Sciences; McGill University Freedman, Miriam; The Pennsylvania State University, Chemistry

ARTICLE

Experimental Phase Diagram and Its Temporal Evolution for Submicron 2-Methylglutaric Acid and Ammonium Sulfate Aerosol Particles

Received 00th January 20xx,
Accepted 00th January 20xx

DOI: 10.1039/x0xx00000x

Qishen Huang[a,b], Kiran R. Pitta[a], Kayla Constantini[a], Emily-Jean E. Ott[a], Andreas Zuend[c], and Miriam Arak Freedman*[a,d]

Liquid–liquid phase separation (LLPS) in aerosol particles is important for the climate system due to its potential to impact heterogeneous chemistry, cloud condensation nuclei, and new particle growth. Our group and others have shown a lower separation relative humidity for submicron particles, but whether the suppression is due to thermodynamics or kinetics is unclear. Herein, we characterize the experimental LLPS phase diagram of submicron 2-methylglutaric acid and ammonium sulfate aerosol particles and compare it to that of supermicron-sized particles. Surprisingly, as the equilibration time of submicron-sized aerosol particles was increased from 20 min to 60 min, the experimental phase diagram converges with the results for supermicron-sized particles. Our findings indicate that nucleation kinetics are responsible for the observed lower separation relative humidities in submicron aerosol particles. Therefore, experiments and models that investigate atmospheric processes of organic aerosol particles may need to consider the temporal evolution of aerosol LLPS.

Introduction

Atmospheric aerosol particles containing both organic compounds and inorganic salts are abundant in the atmosphere, and have a significant effect on chemical and physical processes in the atmosphere, including those that impact human health and climate.[1] The properties of aerosol particles and their temporal evolution dictate the phase state of aerosol particles, which can influence their climate and health effects.[1–5] As the relative humidity (RH), and thereby also the aerosol water activity, changes in the atmosphere, one of the most important phase transitions for organic aerosol particles is liquid–liquid phase separation (LLPS). The occurrence of LLPS leads to the formation of two phases with different solubilities: an organic-rich phase and an inorganic-rich phase. The two phases often have high water activity at the separation relative humidity (SRH) as the SRH is generally relatively high (>70% RH).[1,2,6]
LLPS can impact heterogeneous chemistry, cloud condensation nucleus formation, and new particle growth in the atmosphere, and thus is important to atmospheric chemistry and physics.[1] The occurrence of LLPS as well as the SRH involve the formation of an interface, which can be affected by aerosol physiochemical properties such as chemical composition,[7,8] pH,[9–12] and the size of the aerosol particles.[13,14] Characterization of the effects of aerosol properties on LLPS requires techniques that can characterize aerosol phase separation and SRH. Commonly used methods include microscopy and spectroscopy, with droplets either on a substrate or levitated.[15–17] Most studies that characterize the separation relative humidity (SRH) at which LLPS occurs are performed on particles tens to hundreds of micrometers in diameter. The measured SRH values are often in agreement with thermodynamic model predictions. However, only limited data are available to study LLPS of submicron aerosol particles. In the atmosphere, submicron aerosol particles are arguably more abundant than micrometer-sized droplets; furthermore, aerosol LLPS can impact the global radiation via changes in aerosol optical properties[18] and affect cloud condensation nuclei activation via impact on aerosol surface tension.[19–22] Therefore, a better understanding of LLPS of submicron aerosol is significant to understand the limiting factors for new phase formation in confined nanometer-sized systems, which in turn provide implications for atmospheric chemical and physical processes that can optimize model predictions.[23–25] Our group and other researchers have shown that SRH for submicron particles tends to occur at lower relative humidities and over a larger range of values than measured for micrometer-sized droplets.[14,26,27] It is unclear whether these differences are due to thermodynamics or kinetics. Thermodynamic equilibrium computations accounting for LLPS based on the Aerosol Inorganic–Organic Mixtures Functional groups Activity Coefficient (AIOMFAC) model for nonideal mixing, hereafter referred to as AIOMFAC-LLE, show that the SRH of organic–inorganic aerosols usually has

[a] Department of Chemistry, The Pennsylvania State University, University Park, Pennsylvania 16802, United States.
[b] Institute of Chemical Physics, School of Chemistry and Chemical Engineering, Beijing Institute of Technology, Beijing, 100081, China.
[c] Department of Atmospheric and Oceanic Sciences, McGill University, Montreal, Quebec, H3A 0B9, Canada.
[d] Department of Meteorology and Atmospheric Science, The Pennsylvania State University, University Park, Pennsylvania 16802, United States.
[e] Electronic Supplementary Information (ESI) available: Experimental methods, additional experimental data(size distribution of particles, optical images of micrometer droplet, ERH of submicron inorganic particles), and AIOMFAC prediction of the viscosity of 2MGA+AS aerosols. See DOI: 10.1039/x0xx00000x

a consistent value across a wide range of the dry mass fraction of the inorganic component.[25,28–31] At both low and high inorganic dry mass fractions, in many relevant aerosol systems, the SRH decreases drastically until LLPS is inhibited since a single liquid phase becomes the stable (favored) state.[24,32] Moreover, LLPS can occur spontaneously at the critical point of the system where no energy barrier exists that might otherwise delay or prevent the phase transition from occurring. The phase diagram of LLPS features an unstable region marked by the spinodal curve, which, once reached, allows for barrier-free LLPS, not just in the vicinity of the critical point. However, if one is sufficiently far away from the critical point, the RH of the spinodal curve can be substantially lower than that of the binodal curve.[31,32] To determine the phase diagram for LLPS, SRH values for the plateau region of the binodal curve, the sloping downward region, and the region near the critical point need to be characterized (see Fig. 3a for an example, discussed below).

Our lab has developed a flash-freeze flow tube coupled with cryogenic-transmission electron microscopy (cryo-TEM) that can characterize phase transitions of submicron aerosol particles and measure SRH.[33] Using cryo-TEM, we have shown the suppression of SRH in submicron aerosol particles and that LLPS is inhibited in aerosol particles that are sufficiently small, with the size threshold dependent on the drying rate.[13,26,34,35] In this study, we conducted experiments to construct the room-temperature phase diagram of LLPS in model submicron aerosol particles composed of 2-methylglutaric acid and ammonium sulfate (2MGA+AS) to achieve a deeper understanding of submicron aerosol LLPS. We compared this submicron phase diagram with the experimental phase diagram of LLPS in micrometer droplets determined with optical microscopy as well as thermodynamic calculations made with AIOMFAC-LLE for the macroscopic system. To determine the phase diagram of submicron aerosol LLPS, we studied the 2MGA+AS system systematically by varying the AS dry mass fraction (mf_d(AS)) of the aerosol particles, equilibrating at different RH values, and then characterizing the aerosol morphology (phase separated or homogeneous) for images collected using cryo-TEM.

Experimental

Separation relative humidity (SRH) of micrometer droplets

The SRH values of micrometer droplets were measured using a Nikon Ti2 inverted microscope (20× objective) paired with an environmental chamber. Following deposition, droplets were brought to efflorescence by decreasing the RH to ~25% and then humidified to deliquescence and equilibrated at ~95% for 15 min to ensure equilibrium. The RH was changed at a rate of ~1 %/min, and the SRH was calculated as the mean value of 30 droplets. The detailed procedure can be found in our previous studies.[26]

Aerosol Generation

We generated aerosol particles from aqueous mixtures of 2-methylglutaric acid (2MGA) and ammonium sulfate (AS) with various mass fractions (in terms of dry mass, mf_d(AS)). The solution contained 0.05 wt.% of total solute, and the mf_d(AS) were 0.10, 0.20, 0.47, 0.50, 0.55, 0.80, and 0.90. The aerosol particles were generated using a constant output atomizer (TSI 3076, TSI Inc.).

Dry Aerosol Collection

A diffusion dryer was used to dry the generated aerosols to < 2% relative humidity (RH) with a high drying rate (~99.7%RH/s). A miniMOUDI cascade impactor (TSI 135-8A) was used to collect the particles on 200 mesh copper grids with a carbon film (Electron Microscopy Sciences, CF200-CU). Samples were stored in a desiccator and imaged within 24 hrs. More details can be found in our previous studies.[36]

Aerosol Equilibration and Collection at fixed RH

Aerosol particles were equilibrated at fixed RH, vitrified in a flash-freeze flow tube, and impacted onto TEM grids, as described in our previous study.[26,33] Briefly, a Tedlar bag (~ 500 L) was filled with the generated particles (~98 % RH). We decreased the RH in the bag at a rate of ~0.5 % RH/min with ultra-purified nitrogen gas to adjust the RH in the bag. We measured the particle number concentration using a condensation particle counter (CPC, TSI model 3752) and RH using a RH and temperature probe (Vaisala HMP 110, instrumental error ±1.5%RH[33]). As recorded by the Vaisala HMP 110, all measurements were conducted within the temperature range of 297±1 K. Particles were equilibrated at the desired RH for 20 mins before collection unless otherwise stated. On average, the final particle concentration was between 6×10^3 – 4×10^4 particles/cm^3. Particles were collected on carbon film coated copper TEM grids (Electron Microscopy Sciences, CF200-CU) at a rate of 2.5 LPM.[33] The samples were transferred into liquid nitrogen to remain frozen and to prevent exposure to moisture.

Imaging with Cryogenic Transmission Electron Microscopy

The TEM grids were transferred to a Gatan cryo-holder under liquid nitrogen. The particles were imaged at -175 ºC using either a FEI Talos C TEM with a 200 kV electron beam and cryo-box, or a FEI Tecnai Lab6 TEM with a 200 kV electron beam.

AIOMFAC predictions

The AIOMFAC (Aerosol Inorganic–Organic Mixture Functional groups Activity Coefficients) model has been developed to calculate nonideal mixing in atmospheric aerosols and accounts for interactions between organic functional groups, water and inorganic ions. The model combines a Pitzer-like electrolyte solution model with a UNIFAC-based group contribution approach.[28–30] The AIOMFAC-LLE model is an equilibrium thermodynamics model built as an extension of AIOMFAC,[25] designed to calculate the LLPS of mixed organic–inorganic aerosol systems (solving a system of equations and associated Gibbs energy minimization for the macroscopic "bulk" equilibrium case). To calculate the phase diagram, we input the parameters describing the organic and inorganic compounds according to their functional groups and ion composition, respectively. The model can generate the phase diagram of LLPS by computing the organic–inorganic equilibrium phase compositions for the whole range of mf_d(AS) from high to low

water contents, providing also corresponding water activities, which are equivalent to RH for macroscopic systems.

Results and discussion

Morphology of dry submicron aerosols

Dry submicron aerosol particles with different mf_d(AS) were generated using an atomizer and diffusion drier and imaged with cryo-TEM. Figure 1a shows the morphology of dry 2MGA+AS particles at different mf_d(AS). Particles with apparent contrast between the inner phase and the outer phase, as well as particles with a well-defined phase boundary, are characterized as phase-separated particles. Red arrows in Figure 1a indicate phase boundaries. The image of mf_d(AS) = 0.10 contains one phase-separated particle and a homogeneous particle. One red arrow points to the phase boundary of the phase-separated particle, and the homogenous particle with no phase boundary is presented for comparison. Images of dry aerosol particles show that for mf_d(AS) = 0.20, 0.80, and 0.90, all particles were found to be phase-separated, whereas for mf_d(AS) = 0.10, about 26% of particles were phase-separated, and for mf_d(AS) = 0.95 about 67% of particles were phase-separated. At mf_d(AS) = 0.98, almost all particles were homogeneous. This result suggests that mf_d(AS) = 0.1 and 0.98 are in the region where the binodal curve slopes downwards, and that at slightly smaller or larger mf_d(AS), respectively, no phase separation would be observed. We investigated the size effect of LLPS for particles with mf_d(AS) = 0.33. We imaged over 850 particles and found that LLPS was suppressed when particle size < 100 nm and was inhibited when particle size < 30 nm (Figure S1). This size effect is consistent with our previous observations of the size dependence of the morphology based on drying rate (~99.7% RH/s for this measurement).[34]

LLPS of submicron aerosols at different RH

We characterized the LLPS of 2MGA+AS aerosol particles at different RH and various mf_d(AS) values (0.20, 0.47, 0.50, 0.55, 0.80, and 0.90) via the flash-freeze flow tube coupled to cryo-TEM. Figure 1b shows example images of phase-separated aerosol particles (mf_d(AS) = 0.20) at different RH. We selected different morphologies to display in Figure 1b to show many examples of particle morphologies. Figure 1b(i)&(ii) are similar particles with an inner phase boundary (pointed out by the red arrows). The phase boundary in (i) is close to the edge of the particle, which is of a partially engulfed morphology, whereas the phase boundary in (ii) encloses a core of an inner phase. The majority of particles larger than ~200 nm have similar morphology to either (i) or (ii) across all mf_d(AS) values and RH values. Images (iv), (vii), and (viii) are common morphologies for particles that are smaller than 200 nm with inner phase boundaries. Figure 1b(iii) has an organic-rich phase (light gray) and an inorganic-rich core phase (darker gray). Figure 1b(v) shows an overlay between an organic-rich phase (light gray) and an inorganic-rich core phase (darker gray) which may be due to either inclusion of organic compounds inside the inorganic-rich phase or heterogeneity in the thickness of the organic-rich shell. The inorganic-rich phase in Figure 1b(vi) which was collected at 50% RH, is darker than other images in Figure 1b. The contrast of TEM images, which refers to the darkness of the sample, can be affected by the thickness of the specimen, the atomic number Z (i.e., the mass of the element in the sample), and Bragg diffraction in the crystalline area. A previous study observed that the AS in 1,2,6-hexanetriol/AS droplets started to form a more concentrated inclusion inside the commonly observed AS-rich phase at around 65% RH.[16] The study also showed that at ~50% RH, AS may start to crystallize while the organic-rich phase remains aqueous. Therefore, the darker inorganic phase in Figure1b(vi) may be attributed to a more concentrated AS inclusion at these lower RH values.

Figure 2 depicts LLPS at different RHs for particles sizes between 20 nm and 1 µm. We used the equivalent circular diameter (ECD), which can also be referred as the area equivalent diameter, to represent the particle size. The ECD was calculated according to the particle area from the TEM image with the assumption that particles are spherical. We discussed the

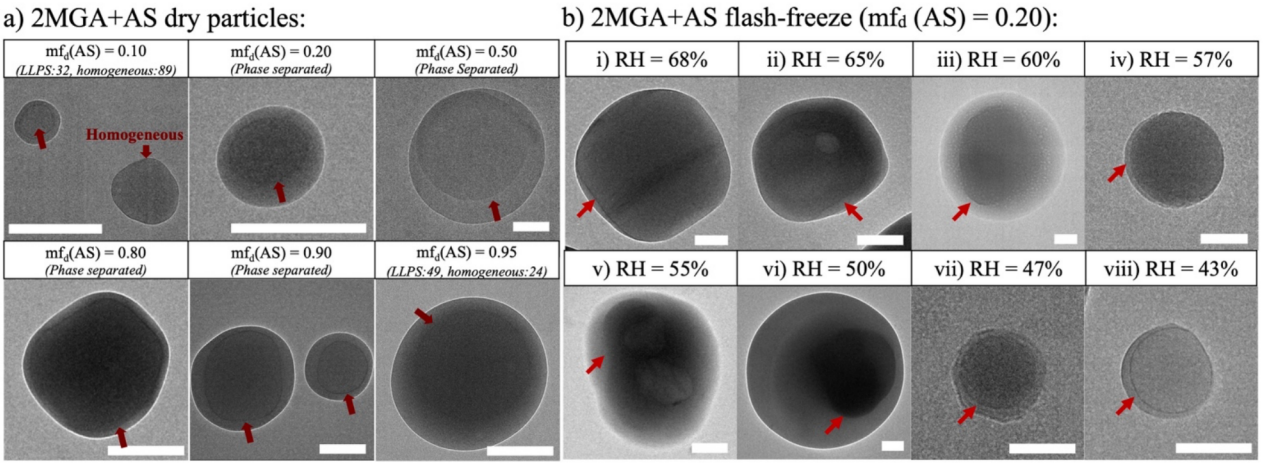

Figure 1 a) The morphology of 2MGA+AS aerosol particles generated at ~297 ± 1 K and dried with a high drying rate (~99.7% RH/s) using the diffusion drier and analyzed using cryo-TEM at different dry mass fractions of AS (mf_d(AS)). For mf_d(AS) = 0.10 and 0.95, not all dry particles (> 100nm) are phase-separated, some of the particles remain homogeneous. b) Example images of particles that have undergone liquid–liquid phase separation (LLPS) when mf_d(AS) = 0.20 at different RH values. Red arrows indicate the phase boundary between the organic-rich and the inorganic-rich phase. Scale bar = 100 nm.

difference in the measured particle size between TEM and scanning mobility particle size spectrometry in our recent work.[37] All data points were collected at 297 ± 1 K and with a 20 min equilibration time. Previous studies assessed that submicron aerosol particles can reach equilibrium within 1 μs when considering water condensation and diffusion.[38] If considering the gas–particle partitioning of semi volatile organic compounds (e.g., 2MGA) and the liquid–liquid equilibrium in LLPS particles, the overall time scale of equilibration should be longer than 1 μs and may be even longer than seconds.[8,39] In this study, given the relatively low solute concentration and low viscosity (~$10^{-2.0\pm0.5}$ Pa·s estimated by AIOMFAC at ~78% RH and 298K, see details in Table S2) in 2MGA+AS aerosols, the 20 min equilibration time should provide a typical SRH value of submicron aerosol LLPS. At mf_d(AS) values that are away from the critical point, all particles were homogeneous (red dots) at high RH. At intermediate RH, the observed particles showed a mixture of morphologies, some are homogeneous (red dots) and others are phase-separated (blue diamonds). At low RH, all particles > 100 nm were phase-separated (all blue diamonds) and particles < 30 nm remained homogeneous (all red dots). This indicates that from high RH to low RH, particles changed from homogeneous to phase-separated, in part depending on size. Similar to dry particles, the LLPS was suppressed when the particle size was smaller than 100 nm and was inhibited when the particle size was smaller than 30 nm. For mf_d(AS) values that are close to the critical point, the majority of particles phase separated at RH values as high as 88%, which is the highest RH level studied in our experimental setup. The inhibition of LLPS is also observed in these groups.

We can define the average SRH for submicron aerosols at each mf_d(AS) using the average RH value of all phase-separated particles until the first complete phase separation ($SRH = \sum_{i=1}^{n_{LLPS}} RH(i)/n_{LLPS}$, where n_{LLPS} is the number of phase-separated particles). When mf_d(AS) values are close to the critical point, if complete LLPS occurs spontaneously at the highest attainable RH, we use the highest RH as the SRH. We validated the RH measurement by measuring the efflorescence RH (ERH) of previously studied systems (KCl and K_2SO_4).[40] The measured ERH agrees well with the literature reported values (Table S1). With the set of average SRH values for each mf_d(AS) we can estimate the LLPS phase diagram of submicron 2MGA+AS aerosols.

Phase diagram of micrometer droplets

To better interpret the submicron phase diagram, we investigated the LLPS of 2MGA+AS micrometer droplets using optical microscopy (Figure S2) and AIOMFAC-LLE predictions. We constructed the phase diagram for micrometer droplets using the SRH values measured at different mf_d(AS) (red line, Figure 3a). For optical microscopy measurements, if the activation barrier for the phase separation process is low, the SRH values should give an indication of the approximate position of the binodal curve. We compared our experimental phase diagram to the predicted one from the AIOMFAC-LLE

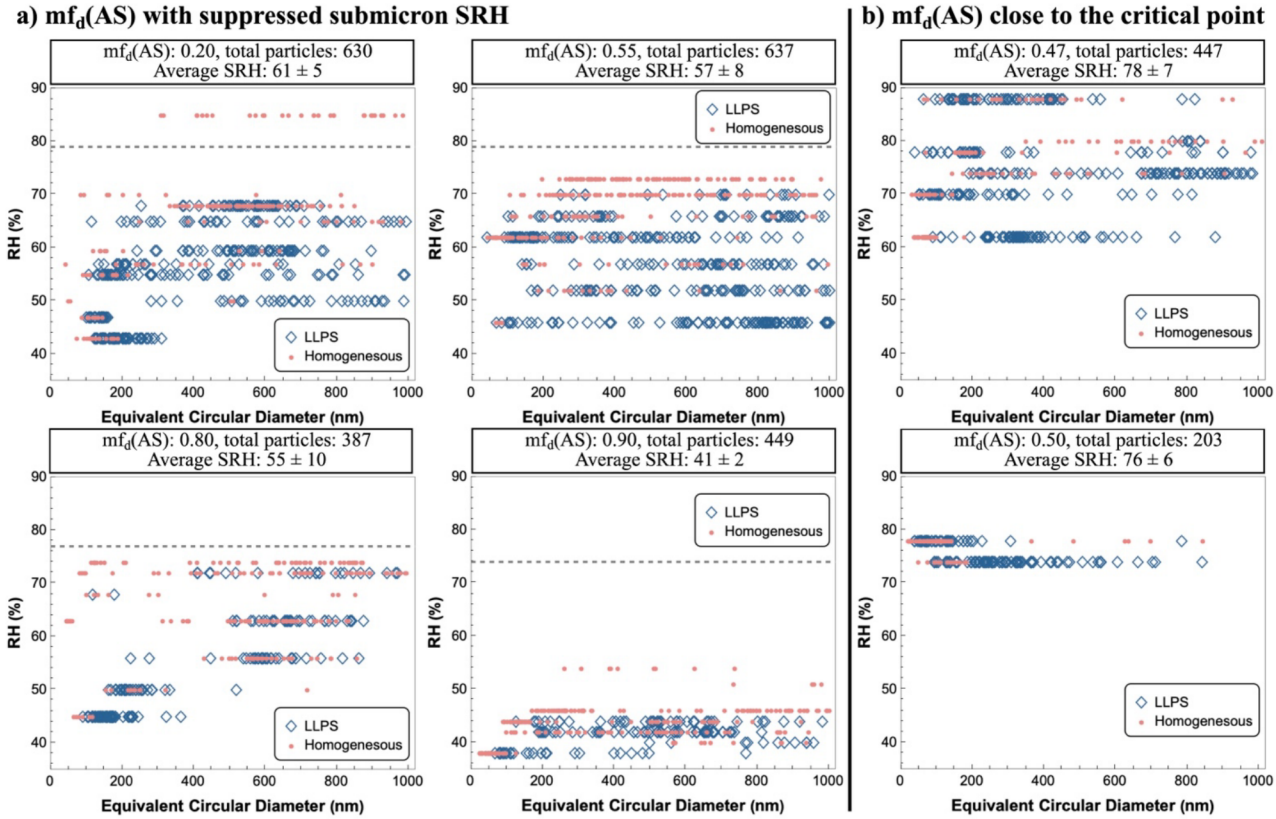

Figure 2. a) Summary of LLPS (blue diamonds) vs. homogeneous (red dots) with mf_d(AS) values that are away from the critical point. The gray dashed line represents the SRH of micrometer droplets measured via optical microscopy. b) Summary of LLPS (blue diamonds) vs. homogeneous (red dots) particles at mf_d(AS) values near the critical point. Each marker represents a single particle. All data points were collected at 297 ± 1 K.

calculations (Figure 3a). The estimated (experimental) binodal curve is comparable with the AIOMFAC-LLE calculations when mf_d(AS) > 0.30. At some mf_d(AS) values the measured SRH is ~3% lower than the AIOMFAC-LLE prediction. This difference is within the range of the instrumental error of the RH probe; also, AIOMFAC-LLE predictions of SRH may be high-biased by a few % in RH. The downward region at high mf_d(AS) (> 0.90) is hard to capture experimentally due to the acute change in the binodal curve, thus the experimental results are considered similar to the AIOMFAC-LLE predictions. In the low mf_d(AS) region (< 0.30), the AIOMFAC-LLE model predicts a large change toward lower RH at mf_d(AS) ~ 0.27, which is higher than what we observed using the optical microscope (between mf_d(AS) = 0.15 and 0.20). The predictions from the AIOMFAC-LLE model are made using a group-contribution-based functional group representation of organic compounds (and inorganic compounds), with various parameters accounting for the interactions among the groups in a solution. This approach is versatile and offers a degree of predictability for a wide range of multicomponent systems; however, for any particular system or organic compound, limitations in the accuracy of the group-contribution approach can impact the precise phase compositions and phase boundaries computed for LLPS. [30] In the ternary system from this work, deviations between the model predictions and the experimental binodal appear to be most obvious for either low or high values of mf_d(AS).[28–30]

Phase diagram of submicron aerosol particles

As shown in Figure 3, we generated the phase diagram of LLPS for submicron aerosol particles from our measurements of 2MGA+AS aerosol particles (blue dashed line) by interpolating the average SRH values at different mf_d(AS) that are away from the critical point (i.e., 0.10, 0.20, 0.33, 0.80, 0.90, 0.98). Note that the average SRH for mf_d(AS) = 0.33 is from our previous study.[26] The upper bound of the shaded area denotes the onset of LLPS (binodal curve), and the lower bound may in part coincide with the spinodal curve for submicron particles in the composition space sufficiently far away from the critical point where all particles are phase-separated below this curve. Figure 3a shows that the shape of the phase diagram of submicron aerosol is similar to that of micrometer-sized droplets. For the phase diagram of submicron aerosols, both the onset SRH and the average SRH of LLPS were suppressed compared to micrometer droplets when mf_d(AS) ranged from 0.20 to 0.90. The mf_d(AS) values that are close to the critical point (0.45, 0.47, 0.50) represent the region at and near spontaneous phase separation (black dots in Figure 3a&b) with average SRH values that ranged from 76% to 81%. The result in the vicinity of the critical point is consistent with both the AIOMFAC-LLE prediction and our previous observations (mf_d (AS) = 0.45).[26] The submicron phase diagram enters the region where SRH falls rapidly as a function of mf_d(AS) when mf_d(AS) is < 0.20 and > 0.90. This result coincides with the experimental phase diagram for micrometer droplets, and suggests that the particle size has a negligible effect on shifting the region where SRH decreases rapidly with mf_d(AS), i.e., the composition space within which phase separation starts to be inhibited thermodynamically.

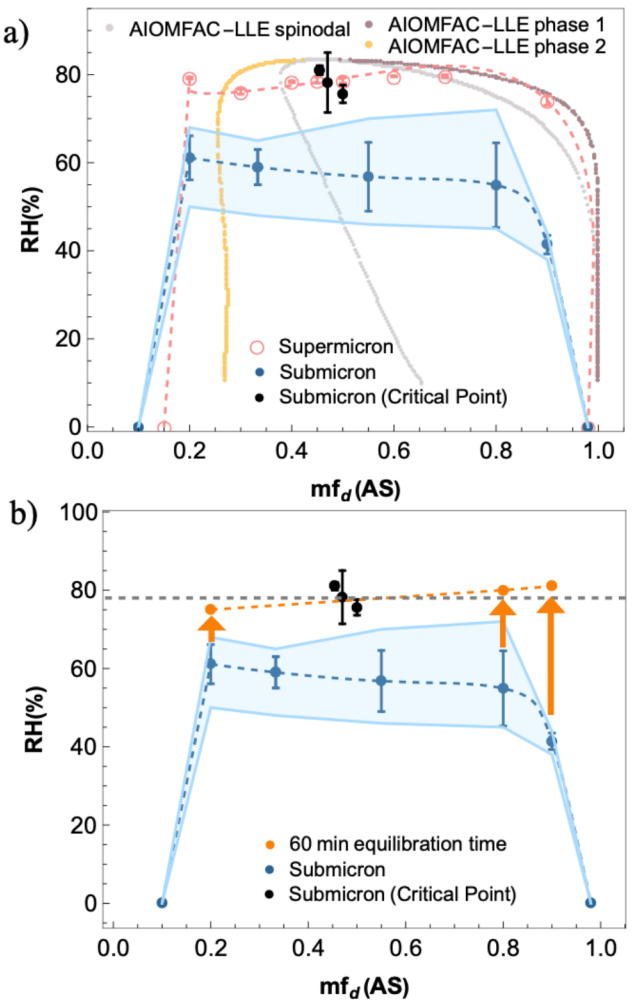

Figure 3. a) The LLPS phase diagram of the 2MGA+AS system with a 20 min equilibration time containing: i) the AIOMFAC-LLE predicted phase diagram which is composed of two curves: a binodal curve (part 1 in yellow and part 2 in violet), and a spinodal curve (grey); ii) the measured LLPS phase diagram of micrometer-sized 2MGA+AS droplets (red line), each data point is the mean value of 30 droplets; iii) the LLPS phase diagram of submicron 2MGA+AS aerosol particles. The shaded area denotes the onset RH of LLPS (upper boundary) and the RH where aerosol particles were entirely phase-separated (lower boundary); and iv) the black points are near the critical point where 2MGA+AS aerosol particles spontaneously phase separate. b) The change of the LLPS phase diagram after 60 min equilibration time (orange points) analyzed near the SRH found for micrometer droplets. The grey dotted line denotes 78% RH, which is a representative SRH value of micrometer-sized droplets.

The effect of equilibration time

To investigate the role of kinetic factors on the phase diagram for submicron aerosol particles, we conducted flash-freeze experiments with a 60 min equilibration time for mf_d (AS) = 0.20, 0.80, and 0.90 (Figure 3b). We equilibrated and analyzed the captured aerosol particles only near the RH at which SRH occurs for micrometer droplets. These morphologies were compared to the results of aerosol particles with the same compositions but with a 20 min equilibration time (Figure 2a & 3b). The result from mf_d (AS) = 0.20 and 75% RH shows that the inhibition of LLPS in aerosol particles < 30 nm occurs regardless of the equilibration time. Figure 4 shows that for a 20 min

equilibration time, aerosol particles are homogenous at 70%, 74%, and 54% RH for mf_d(AS) = 0.20, 0.80, 0.90, respectively. For 60 min equilibration time, in comparison, most aerosol particles are phase separated at 75% for mf_d(AS) = 0.20, and aerosol particles are completely phase separated at 80%, and 81% RH for mf_d(AS) = 0.80 and 0.90, respectively. Figure 3b depicts the change of the submicron phase diagram with a 60 min equilibration time, the gray dotted line in Figure 3b denotes 78%, which represents the SRH value of supermicron droplets across intermediate mf_d (AS) values. Note that these SRH values would have larger error bars if considering the instrumental error from the RH probe. This instrumental error may account for the fact that some SRH values from the 60 min equilibration experiments (orange points in Figure 3b) are as high or slightly higher compared to AIOMFAC-LLE and the measured SRH of micrometer-sized droplets whereas the SRH at the critical point is usually the highest. Overall, the SRH values of submicron particles are in the same range of SRH as that of micrometer-sized droplets. In our recent study, we examined different equilibration times (5 min, 20 min, 30 min, and 75 min) at mf_d (AS) = 0.33.[26] We found that the 20 min and 30 min groups showed a comparable proportion of phase-separated particles, which is more than that of the 5 min group.[26] Similar to the 60 min observation in this study, aerosol particles were entirely phase-separated when a 75 min equilibration time was used.[26] Combining the results in this study and our previous observations, we can depict the temporal evolution of the phase diagram of the 2MGA+AS system. Our results show that i) with sufficient equilibration time (≥ 60 min) the submicron phase diagram converges with the phase diagram of micrometer-sized droplets, and further lengthening of the equilibration time will not change the phase diagram; ii) with shorter equilibration times, SRH is kinetically suppressed, and the apparent phase diagram (and the binodal curve) is translated to lower relative humidities compared with that of micrometer-sized droplets; and iii) a shorter equilibration time yields a greater suppression of SRH and a phase diagram further translated to lower relative humidities. This result is also likely applicable to many other organic aerosol systems. This result indicates that kinetic effects are dominating the suppression of SRH in submicron aerosol particles, and the thermodynamic effects on SRH are negligible in the studied size range. SRH in micrometer-sized droplets occurs within a time scale of several seconds according to our observations using an optical microscope. For submicron aerosol particles, we observed the convergence of the submicron and micrometer phase diagram with a 60 min equilibration time which indicates that the kinetics of the formation of a new phase are substantially (and surprisingly) limited during LLPS of submicron aerosol particles. The viscosity of 2MGA-AS aerosol particles is expected to be relatively low at SRH, thus should not significantly limit the diffusive growth of the nucleated phase. The formation of a new phase may be limited by the stochastic effect of nucleation in submicron aerosol particles. Submicron particles may have a low probability of nucleation of a new phase in the first 20–30 min, which leads to suppressed SRH, but have a sufficient nucleation rate for 60 min of equilibration. In contrast, the much larger volume in micrometer-sized particles allows for the nucleation of a new liquid phase within a much shorter time span. To further validate the cause of our findings, we will need to design experiments to resolve the origins of the kinetic factors affecting SRH for submicron 2MGA+AS aerosol particles.

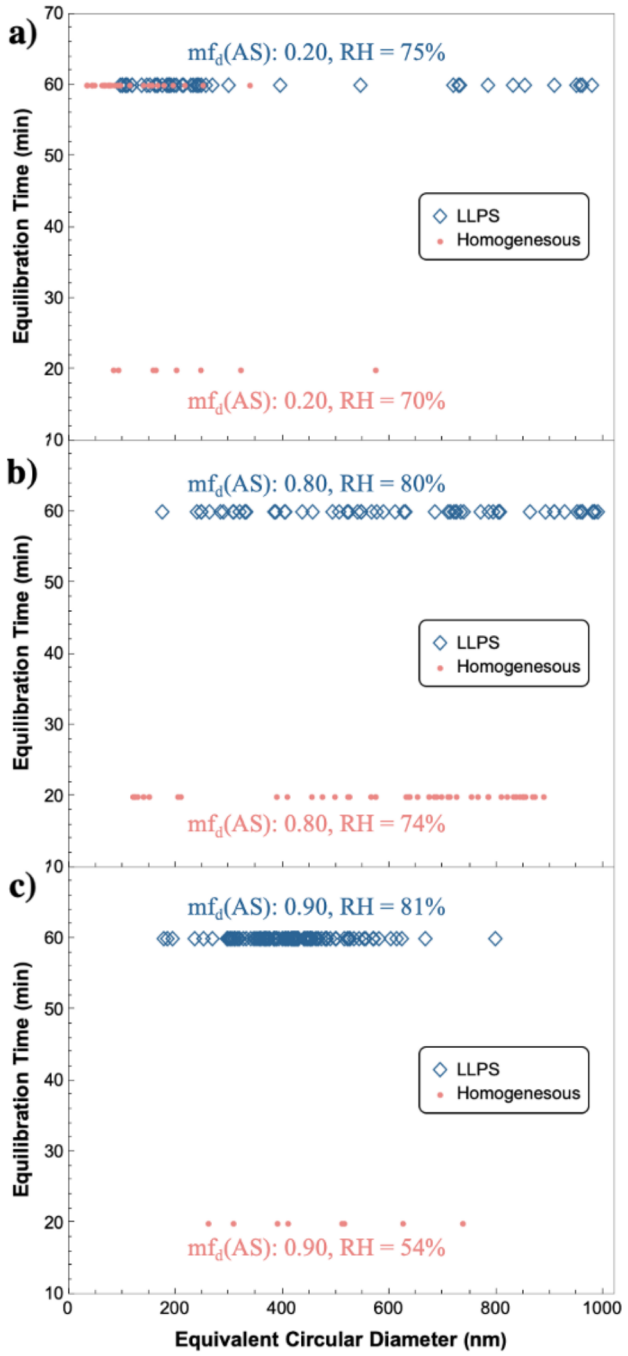

Figure 4 The effect of equilibration time on SRH. a) mf_d (AS) = 0.20: Aerosol particles are homogeneous at 70% RH with a 20 min equilibration time, whereas most aerosol particles are phase separated at 75% RH with a 60 min equilibration time. b) mf_d (AS) = 0.80: Aerosol particles are homogenous at 74% RH with a 20 min equilibration time and are completely phase separated at 80% RH with a 60 min equilibration time. c) mf_d (AS) = 0.90: Aerosol particles are homogenous at 54% RH with a 20 min equilibration time and are completely phase separated at 81% RH with a 60 min equilibration time. All data points were collected at 297 ± 1 K.

Conclusions

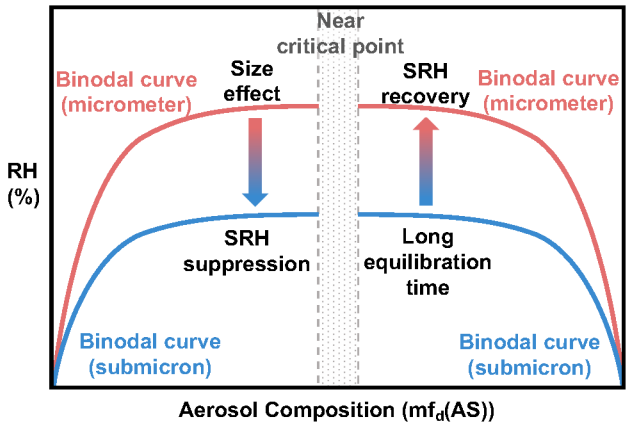

Figure 5 Schematic graph that summarizes the findings of this study.

In summary, we constructed the phase diagram of LLPS for 2MGA+AS submicron aerosol particles. The size of particles ranged from 20 nm to 1 μm. We characterized the SRH of these aerosol particles with 20 min and 60 min equilibration times to investigate the contribution of thermodynamics and kinetics on submicron aerosol LLPS. The experimentally derived phase diagram of 2MGA+AS micrometer-sized droplets agrees well with thermodynamic calculations using the AIOMFAC-LLE model. Figure 5 is a schematic graph that summarizes our experimental observations of measured phase diagrams of submicron aerosols and micrometer-sized droplets. Using a 20 min equilibration time, the SRH for submicron 2MGA+AS aerosol particles is suppressed compared to micrometer droplets except for the region in the composition space that is close to the critical point, since LLPS can occur spontaneously (but not instantaneously) at the critical point. When extending the equilibration time to 60 min, the submicron aerosol phase diagram converges with that of micrometer droplets, which indicates that the suppression of SRH is due to kinetic factors and the formation of a new liquid phase is substantially limited. For aerosol particles that are < 30 nm, LLPS is inhibited. This size dependence shows that LLPS is thermodynamically unfavorable when aerosol particles are sufficiently small, in agreement with our previous work.[34] The dry solute compositions in the phase diagram for which the binodal curve slopes downward are consistent between submicron and supermicron phase diagrams (mf_d(AS) <0.2 and >0.9), indicating that thermodynamics rather than kinetic factors dominate the outcome in these regions. Therefore, for aerosol particles with compositions in this region, we can rely on the microscopic phase diagram and thermodynamic models to predict LLPS. This work provides a detailed phase diagram of submicron 2MGA+AS aerosols and shows the limiting factors for different regions of the phase diagram. Our findings show that when considering the LLPS of a population of organic aerosols, the ambient RH, the chemical composition, and the equilibration time have significant effects. Moreover, we showed that due to kinetic limitations, the equilibration time for submicron aerosol to entirely phase separate is significantly longer than that for micrometer-sized droplets. This result implies that when investigating chemical and physical processes of Aitken and accumulation mode aerosol particles that involve LLPS, via either experiments or modelling, the temporal evolution of the aerosol LLPS during the time scale of the chemical and physical processes need to be considered.

Author Contributions

M.A.F. conceptualized, designed, and supervised the study. Q.H., K.R.P., K.C., and E.-J.E.O. conducted the experiments. Q.H. performed analyses and wrote the original draft. QH., A.Z. and M.A.F. reviewed and edited the manuscript.

Conflicts of interest

The authors declare no competing financial interest.

Acknowledgements

Q. H., K. R. P., K. C., E.-J. E. O., and M. A. F. gratefully acknowledge the support from DOE grant DE-SC0018032. We thank the Materials Characterization Lab (MCL) at Penn State for the use of FEI Talos C TEM and the FEI Tecnai Lab6 TEM, and the Huck Institutes of the Life Sciences for the use of Gatan cryo-holder. We acknowledge J. L. Gray and M. Hazen for their help with TEM imaging. A. Z. acknowledges support by the Natural Sciences and Engineering Research Council of Canada (grant no. RGPIN-2021-02688).

References

1 M. A. Freedman, *Chem. Soc. Rev.*, 2017, **46**, 7694–7705.
2 C. Marcolli and U. K. Krieger, *J. Phys. Chem. A*, 2006, **110**, 1881–1893.
3 Y. You, M. L. Smith, M. Song, S. T. Martin and A. K. Bertram, *Int. Rev. Phys. Chem.*, 2014, **33**, 43–77.
4 A. P. Ault and J. L. Axson, *Anal. Chem.*, 2017, **89**, 430–452.
5 J. H. Seinfeld, S. N. Pandis and K. Noone, *Atmospheric Chemistry and Physics: From Air Pollution to Climate Change*, John Wiley & Sons, NJ, 3rd edn., 2016.
6 S. L. Clegg, J. H. Seinfeld and P. Brimblecombe, *J. Aerosol Sci.*, 2001, **32**, 713–738.
7 Y. You, L. Renbaum-Wolff and A. K. Bertram, *Atmos. Chem. Phys.*, 2013, **13**, 11723–11734.
8 Y. Huang, F. Mahrt, S. Xu, M. Shiraiwa, A. Zuend and A. K. Bertram, *Proc. Natl. Acad. Sci. U. S. A.*, , DOI:10.1073/pnas.2102512118.
9 D. J. Losey, R. G. Parker and M. A. Freedman, *J. Phys. Chem. Lett.*, 2016, **7**, 3861–3865.
10 Y. Tong, X. Meng, B. Zhou, R. Sun, Z. Wu, M. Hu and A. Ye, *Front. Phys.*, 2022, 1–8.
11 Z. Lei, Y. Chen, Y. Zhang, M. E. Cooke, I. R. Ledsky, N. C. Armstrong, N. E. Olson, Z. Zhang, A. Gold, J. D. Surratt and A. P. Ault, *Environ. Sci. Technol.*, 2022, **56**, 10596–10607.
12 D. J. Losey, E. J. E. Ott and M. A. Freedman, *J. Phys. Chem. A*, 2018, **122**, 3819–3828.

13 D. P. Veghte, M. B. Altaf and M. A. Freedman, *J. Am. Chem. Soc.*, 2013, **135**, 16046–16049.
14 T. M. Kucinski, J. N. Dawson and M. A. Freedman, *J. Phys. Chem. Lett.*, 2019, **10**, 6915–6920.
15 Y. You, L. Renbaum-Wolff and A. K. Bertram, *Atmos. Chem. Phys.*, 2013, **13**, 11723–11734.
16 S. Ma, Z. Chen, S. Pang and Y. Zhang, *Atmos. Chem. Phys.*, 2021, **21**, 9705–9717.
17 N. Wang, B. Jing, P. Wang, Z. Wang, J. Li, S. Pang, Y. Zhang and M. Ge, *Environ. Sci. Technol.*, 2019, **53**, 6225–6234.
18 Y. Yao, J. H. Curtis, J. Ching, Z. Zheng and N. Riemer, *Atmos. Chem. Phys.*, 2022, **22**, 9265–9282.
19 J. F. Davies, A. Zuend and K. R. Wilson, *Atmos. Chem. Phys.*, 2019, **19**, 2933–2946.
20 K. Gorkowski, N. M. Donahue and R. C. Sullivan, Aerosol Optical Tweezers Constrain the Morphology Evolution of Liquid-Liquid Phase-Separated Atmospheric Particles.
21 J. Ovadnevaite, A. Zuend, A. Laaksonen, K. J. Sanchez, G. Roberts, D. Ceburnis, S. Decesari, M. Rinaldi, N. Hodas, M. C. Facchini, J. H. Seinfeld and C. O'Dowd, *Nature*, 2017, **546**, 637–641.
22 S. Zhou, B. C. H. Hwang, P. S. J. Lakey, A. Zuend, J. P. D. Abbatt and M. Shiraiwa, *Proc. Natl. Acad. Sci. U. S. A.*, 2019, **116**, 11658–11663.
23 A. Nenes, C. Pilinis and S. N. Pandis., *Aquat. Geochemistry*, 1998, **4**, 123–152.
24 A. Zuend and J. H. Seinfeld, *Atmos. Chem. Phys.*, 2012, **12**, 3857–3882.
25 A. Zuend and J. H. Seinfeld, *Fluid Phase Equilib.*, 2013, **337**, 201–213.
26 T. M. Kucinski, E. J. E. Ott and M. A. Freedman, *J. Phys. Chem. A*, 2021, **125**, 41.
27 P. E. Ohno, Y. Qin, J. Ye, J. Wang, A. K. Bertram and S. T. Martin, *ACS Earth Sp. Chem.*, 2021, **5**, 1223–1232.
28 A. Zuend, C. Marcolli, B. P. Luo and T. Peter, *A thermodynamic model of mixed organic-inorganic aerosols to predict activity coefficients*, 2008, vol. 8.
29 H. Yin, J. Dou, L. Klein, U. K. Krieger, A. Bain, B. J. Wallace, T. C. Preston and A. Zuend, *Atmos. Chem. Phys.*, 2022, **22**, 973–1013.
30 A. Zuend, C. Marcolli, A. M. Booth, D. M. Lienhard, V. Soonsin, U. K. Krieger, D. O. Topping, G. McFiggans, T. Peter and J. H. Seinfeld, *Atmos. Chem. Phys.*, 2011, **11**, 9155–9206.
31 M. B. Altaf, A. Zuend and M. A. Freedman, *Chem. Commun.*, 2016, **52**, 9220–9223.
32 A. Zuend, C. Marcolli, T. Peter and J. H. Seinfeld, *Atmos. Chem. Phys.*, 2010, **10**, 7795–7820.
33 T. M. Kucinski, E. J. E. Ott and M. A. Freedman, *Anal. Chem.*, 2020, **92**, 5207–5213.
34 M. B. Altaf and M. A. Freedman, *J. Phys. Chem. Lett.*, 2017, **8**, 3613–3618.
35 M. A. Freedman, *Acc. Chem. Res.*, 2020, **53**, 1102–1110.
36 E.-J. E. Ott, T. M. Kucinski, J. N. Dawson and M. A. Freedman, *Anal. Chem.*, 2021, **93**, 11347–11356.
37 E. C. Tackman, D. N. Higgins, D. E. Kerecman, E.-J. E. Ott, M. V. Johnston and M. A. Freedman, *Aerosol Sci. Technol.*, 2023, **57**, 279–295.
38 S. O'Meara, D. O. Topping and G. McFiggans, *Atmos. Chem. Phys.*, 2016, **16**, 5299–5313.
39 M. Shiraiwa, A. Zuend, A. K. Bertram and J. H. Seinfeld, *Phys. Chem. Chem. Phys.*, 2013, **15**, 11441–11453.
40 H. S. Morris, A. D. Estillore, O. Laskina, V. H. Grassian and A. V. Tivanski, *Anal. Chem.*, 2016, **88**, 3647–3654.